

Patient-Specific Finite-Element Simulation of the Insertion of Guidewire During an EVAR Procedure: Guidewire Position Prediction Validation on 28 Cases

J. Gindre*, A. Bel-Brunon, M. Rochette, A. Lucas, A. Kaladji, P. Haigron, and A. Combescure

Abstract—Objective: Validation of a numerical method to compute arterial deformations under the insertion of an "extra-siff" guidewire during Endovascular Repair of Abdominal Aortic Aneurysm. Methods: We propose the validation of a previously developed simulation method. The model is calibrated using anatomical hypothesis and intraoperative observations. Simulation results are blindly evaluated against 3-D imaging data acquired during the surgical procedure on 28 patients, based on the predicted position of the intraoperative guidewire. Results: Simulation was successfully conducted on the 28 patients. The mean position error given by the Modified Hausdorff Distance for the 28 cases was 3.8 \pm 1.9 mm, which demonstrates very good results for most of the cases. Conclusion: The work reported here shows that numerical simulation can predict some rather large variations in the vascular geometry due to tools insertion, for a wide variety of aorto-iliac morphologies. This is a new step toward clinically applicable mechanical simulation. Significance: Validation on 3-D intraoperative data on a large number of cases—robustness on adverse anatomies.

Index Terms—Abdominal aortic aneurysm, 3-D intraoperative data, endovascular aneurysm repair (EVAR), guidewire, patient specific.

I. INTRODUCTION

NDOVASCULAR aneurysm repair (EVAR) is a minimus invasive technique that is commonly used to treat abdominal aortic aneurysms (AAA). It relies on the exclusion of the aneurysm sac by introducing one or more stent-grafts through

Manuscript received January 20, 2016; accepted June 25, 2016. Date of publication July 7, 2016; date of current version April 18, 2017. *Asterisk indicates corresponding author.*

'J. Gindre is with the INSA-Lyon, LaMCoS CNRS UMR5259, F-69621, France and also with the , Université de Rennes 1, LTSI, Rennes F-35000, France and with INSERM U1099, Rennes F-35000, France and , ANSYS, Villeurbanne, F-69100, France (e-mail: juliette.gindre@gmail.com).

A. Bel-Brunon and A. Combescure are with the INSA-Lyon, LaMCoS CNRS UMR5259.

M. Rochette is with ANSYS.

A. Lucas and A. Kaladji are with the Université de Rennes 1, LTSI and with , INSERM, U1099 and also with the University Hospital of Rennes, France.

P. Haigron is with the Université de Rennes 1, LTSI, Rennes F-35000, France and with , INSERM, U1099, Rennes F-35000, France. Digital Object Identifier 10.1109/TBME.2016.2587362

site: first, highly flexible guidewires and catheters which adapt to the arterial lumen, then "extra-stiff" guidewires which purpose is to facilitate the passage of and provide support for the stent-graft introducer, in particular, by straightening the often tortuous iliac arteries. The insertion of these tools induces significant deformations to the vascular structure. These deformations can have clinical consequences and must be accounted for, first at the planning step, and then, during the procedure.

In the preoperative planning, the surgeon must chose the stent-graft model and sizes to ensure that the aneurysm is completely

the femoral arteries and deploying them inside the aneurysm.

During the procedure, several tools of varying stiffness are intro-

duced to enable the delivery of the stent graft to its deployment

In the preoperative planning, the surgeon must chose the stent-graft model and sizes to ensure that the aneurysm is completely sealed without covering important collateral arteries, particularly renal arteries at the proximal landing zone and internal iliac arteries at the distal landing zone. Currently available planning softwares allow stent-graft sizing based on geometrical measurements, lengths and diameters, that are made on the patient preoperative CT-scan. However, the insertion of stiff wires and delivery systems can generate important changes in arterial angulation and lengths that often call into question the relevance and accuracy of previously made measurements.

Then, during the procedure, tools insertion and stent-graft deployment are usually performed under 2-D fluoroscopic imaging, which enables visualization of bones structures and radiopaque tools. Recently, advanced imaging systems have been developed, which allow the fusion of CTA images with live fluoroscopy that can then be used as an arterial roadmap to facilitate endovascular navigation [1]. Such features are increasingly used for EVAR or other complex endovascular interventions [2]–[4]. Yet some authors pointed out that the relevance of fusion is often called into question as soon as stiff devices have deformed the vascular structure, as the preoperative CT-scan does not reflect anymore the current arterial geometry [5]–[7].

Today, to estimate the intraoperative vascular configuration, surgeons must anticipate these deformations based on their experience only. Being able to predict them based on mechanical calculation could bring more objective and useful indicators to prepare the intervention and guide the procedure.

A few previous publications proposed a biomechanical model and a method to predict the deformations caused by guidewire

insertion during EVAR procedure [8]–[10]. Among them, only one study presented an evaluation of the results against quantitative patient-specific intraoperative data [11]. However, the evaluation of the model was based on the projection of the simulation results on a single 2-D image, which is not sufficient to assess the accuracy of 3-D position and shape of the guidewire. Moreover, the simulation method, which was based on implicit finite-element computation, faced convergence difficulties on complex, i.e., tortuous anatomies, which may be the most interesting for clinical applications. In a previous work, we presented a method for the mechanical simulation of the vascular structure deformations due to the insertion of an extra-stiff guidewire during an EVAR procedure using an explicit finite-element software [12]. In this publication, numerical convergence of the model was established, a sensitivity study was presented and a first parametrization of the model was done on one patient case. To our knowledge, this paper also offers the first numerical framework for tools insertion on a whole femoral to aortic arch vascular structure taking into account blood pressure pretension and external support modeling and is, therefore, a first step towards the simulation of the complete process of stent-graft deployment which is an important current subject of research [13], [14].

In the present paper, we focus on the calibration and the validation of this mechanical simulation based on 3-D imaging data acquired during the surgical procedure on 28 patient cases, presenting a wide variety of arterial morphologies, tortuosity levels, and calcification states. As the number of parameters is important and the simulation time is long, the calibration cannot be done with standard automatic optimization methods. Rather, we estimate optimal values based on experience gained through anatomical observations and comparison of the simulation results to the intraoperative reality. The obtained calibration is then blindly evaluated on the 28 patient cases by comparing the position of the guidewire predicted by the simulation to the real intraoperative 3-D position extracted from fluoroscopy images acquired during the surgical procedure.

II. METHODS

A. Clinical Summary

Twenty-eight patients with AAA, who underwent EVAR in the vascular surgery unit of the University Hospital of Rennes, France between February 2012 and January 2015, were included in this study. For each patient, preoperative CTA data and intraoperative fluoroscopy data were obtained. The study protocol was approved by the institutional review board. Patients' informed consent was obtained for being registered anonymously in the database. As described in [12], all preoperative CTA are processed using ENDOSIZE commercial sizing software (Therenva, Rennes, France) to extract a segmentation of arterial lumen and data needed to build the finite-element model: a map of distance between the arterial wall and the spine, a map of arterial wall density, and specific anatomic points like collateral arteries origin and sizing points.

In order to gain insight into the anatomical variability among the considered cases, for each patient we compute five anatomical descriptors of the aorto-iliac morphology. The tortuosity index is computed as the centerline length of the iliac segment divided by the length of the straight line between aortic bifurcation and femoral bifurcation, as introduced in [15]. As proposed in the same publication, iliac calcification is usually graded subjectively by the surgeon between grades 0 and 3. Here, as a more objective quantification method, we compute the calcification percentage as the ratio of calcified surface area on total surface area of iliac artery. Presence of thrombus may have an implication on the mechanical behavior of the wall particularly in case of important thickness. We define the indicator of thrombus thickness as the maximal thickness of intraluminal thrombus measured on cross sections of the vascular structure along the lumen centerline. We define the aortic angle as the minimal angle encountered along the vessel centerline from the beginning of the descending aorta to the aortic bifurcation. In standard grading systems, aortic angle is usually computed as "the most acute angle in the centerline between the lowest renal artery and the aortic bifurcation" [16]. For this study, we extend its definition along the whole descending aorta because we found that angulation above renal arteries can also have consequences on the guidewire position. Finally, the *luminal volume* is automatically computed as the volume corresponding to the arterial lumen between renal arteries and internal iliac arteries origin using a feature of the software EndoSize.

B. Mechanical Model and Simulation Process

The mechanical model and the simulation method were described in a previous publication, thus only main features are briefly recalled here. For more details on the development of the model and the simulation method, the reader is invited to refer to [12].

1) Mechanical Model of the Aorto-Iliac Structure: The vascular geometry represented in the simulations corre-

The vascular geometry represented in the simulations corresponds to an aorto-iliac structure including the abdominal aorta and the common and external iliac arteries. The arterial wall is represented as a surface meshed with triangular shell elements. An homogeneous thickness of 1.5 and 1.2 mm is used respectively on the aorta and on the iliac arteries [12]. The behavior of the wall is modeled using a polynomial, nonlinear, and isotropic hyperelastic potential of Yeoh expressed as a function of the first Cauchy invariant I_1 as follows:

$$W = C_{10} (I_1 - 3) + C_{20} (I_1 - 3)^2$$
 (1)

with $C_{10}=0.005~\mathrm{MPa}$ and $C_{20}=0.2~\mathrm{MPa}$ as proposed in [12]. Elements corresponding to calcification plaques are assigned linear elastic properties (Young's modulus $E=40~\mathrm{MPa}$, Poisson's ratio $\upsilon=0.4$). Collateral arteries are not represented in the geometry, but their mechanical effect is partially taken into account by suitable boundary conditions, as described Section II-B. The surface mesh corresponds to the internal surface of the arterial lumen. Intraluminal thrombus is not represented in the model.

2) External Support: The mechanical support brought by surrounding organs and structures is represented as a viscoelastic surface load on the entire surface of the vascular mesh as

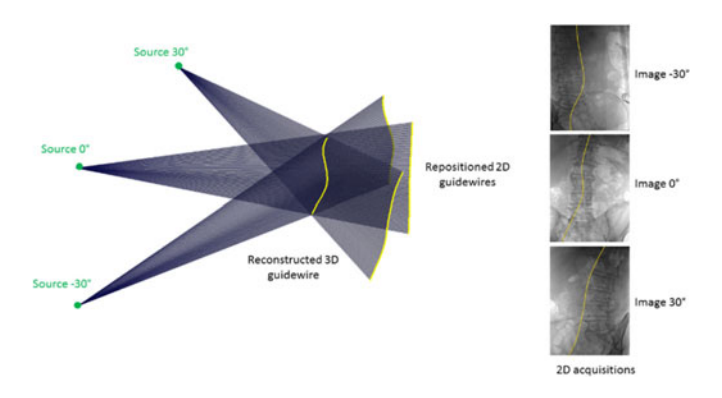


Fig. 1. Three-dimensional guidewire reconstruction process from multi-incidential 2-D images.

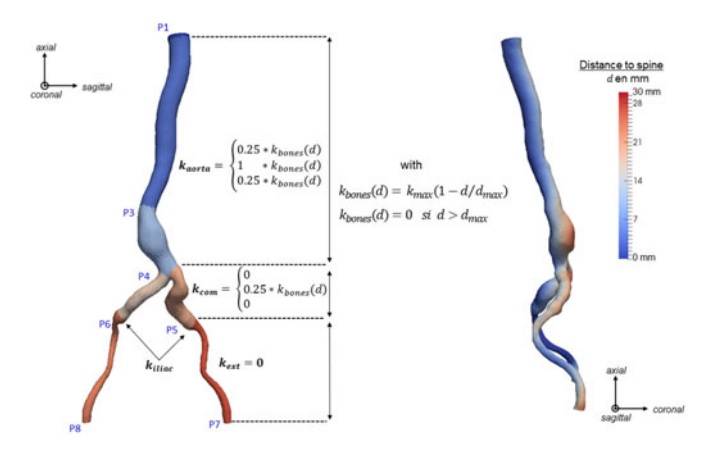


Fig. 2. Illustration of the elastic stiffness distribution of the support.

described in [12]. The elastic part of this load can be expressed at each mesh node by the effort \vec{f}_{ext} expressed as follows:

$$\vec{f}_{ext} = -k\vec{u}.dS \tag{2}$$

where \vec{u} is the displacement of the considered mesh node, k the anisotropic surfacic stiffness coefficient of the support, which depends on global directions and dS an elementary surface.

The stiffness k is proportional to a scalar coefficient $k_{\rm bones}$. $k_{\rm bones}$ is locally defined on the surface of the arterial mesh as a decreasing function of the local distance d from the arterial wall to the spine according to

$$k_{\text{bones}}(d) = k_{\text{max}}(1 - d/d_{\text{max}}) \text{ if } d \le d_{\text{max}}$$

 $k_{\text{bones}}(d) = 0 \text{ if } d > d_{\text{max}}.$ (3)

The stiffness coefficient k is decomposed along the three anatomical directions of the patient: axial, coronal, sagittal, thanks to the scaling factors $\{sf_a, sf_c, sf_s\}$ in order to account for the anisotropy of the support, as defined by

$$\mathbf{k} = \begin{cases} sf_a.k_{\text{bones}}(d) \\ sf_c.k_{\text{bones}}(d) \\ sf_s.k_{\text{bones}}(d) \end{cases}$$
 (4)

The anisotropy factors depend on the location along the vascular structure, which is divided in three segments: the abdominal

aorta, the common iliac arteries, and the external iliac arteries, resulting into three stiffness coefficients $k_{\rm aorta}, k_{\rm com}$, and $k_{\rm ext}$ (see Fig. 2). An isotropic elastic stiffness $k_{\rm iliac} = k_{\rm max}$ is also added at the origin of the internal iliac arteries in order to represent the limited mobility of these points. The relatively stationary proximal and distal extremities are modeled by a zero-displacement condition over the three outer borders of the mesh.

3) Simulation Process: The prestressing effect of blood pressure is included into the model. We use an iterative method similar to the one described in two publications ([17], [18]) to determine a new vascular geometry, which corresponds to a stress-free state often called "zero-pressure" geometry. The internal blood pressure is then applied inside this "zero-pressure" geometry as a static pressure of 75 mmHg, which correspond to a mean level of physiological arterial pressure, to produce the prestressed state of the vascular structure.

After the prestressing step, we proceed with the simulation of guidewire insertion. We first introduce a very soft thin catheter tube meshed with shell elements. The guidewire is then introduced within this tube. The study represents an "extrastiff" Lunderquist (Cook), which is modeled using 189 4-mmlong two-nodes beam elements with linear elastic properties corresponding to standard stainless steel as proposed in [19] (Young's modulus E=180 GPa, Poisson's ratio $\upsilon=0.3$). The guidewire is pushed inside the arterial lumen from the distal end of the external iliac arteries by prescribing a velocity and zero rotation at its lower end until it is fully inserted in the vascular structure. Inside the vascular structure, the guidewire is free. Frictionless contact is assumed with the lumen internal surface. Endovascular tools are designed in order to enhance sliding inside the arteries. Their coefficients of friction are very low, therefore the assumption of frictionless contact seems reasonable.

Several numerical parameters like guidewire insertion velocity, vascular structure, and guidewire discretization, mass-scaling and damping must be tuned to minimize computation time without raising numerical artefacts. All those parameters were subjected to a sensitivity analysis in a previous work along with a mesh convergence study, main results are provided in [12]. In the present paper, we do not reproduce this analysis but simply use the previously determined parameters setting as they are.

The simulation is performed using the Ansys Ls-Dyna Explicit 15.0 finite-element solver on a Dell Precision T7600 workstation equipped with one eight-core Intel-Xeon E5-2687w (3.4 GHz) processor. The mean duration of simulation is 2 h 30 min.

C. Intraoperative Comparison Methodology

1) Registration: For each patient, either a 3-D rotational acquisition or multi-incidence 2-D acquisitions are done with a rotational fluoroscopy imaging system Artis Zeego (Siemens) after the insertion of a Lunderquist "extra-stiff" guidewire (Cook) from the femoral bifurcation up to the aortic arch. When the modality used is multi-incidential 2-D, three images are acquired at angles -30° , 0° , and 30° LAO/RAO. Because preop-

erative and intraoperative data lie into two different coordinate systems, registration must be achieved before any comparison can be done. For both 2-D and 3-D modalities, intraoperative to preoperative rigid registration is done based on bones structure. The registration of 2-D images is done with an intensity-based 3-D/2-D registration method that uses digitally reconstructed radiographs (DRR). The similarity method used to compare the produced DRR to the intraoperative image is based on gradient difference. We use an exhaustive approach to search for the optimal transformation method. The main concepts cited here are defined in [1], the method used is described in more details in [20]. Concerning 3-D acquisitions, interactive registration is achieved under synchronized axial, coronal, and sagittal views with the help of the manual Registration module of MeVis-Lab 2.2.1 open source software (MeVis Medical Solutions AG, Bremen, Germany).

- 2) Segmentation: The region of interest for comparison between intraoperative and simulated guidewire is defined as the portion of guidewire lying axially between renal arteries origin and the femoral artery bifurcation, which corresponds to the maximal path available for deployment of the stent-graft. Thanks to its high density, the guidewire is clearly visible on intraoperative images and can be easily segmented. The segmentation is done by positioning 2-D or 3-D points along the guidewire path, which is then described by a B-spline curve.
- *3) Reconstruction:* For the 3-D images, the tridimensional position of the registered guidewire is directly obtained after the segmentation step. Concerning the 2-D images, the last step consists in reconstructing the 3-D position of the guidewire from the three segmentation curves obtained from -30° , 0° , and 30° LAO/RAO images [21], [22]. To do so, we use the acquisition parameters of the imaging system (source/detector position, calibration parameters) to virtually repositioned the images and the imaging source in the 3-D space to reproduce the geometrical configuration at the time of acquisition. This allows reconstructing the 3-D position of the intraoperative guidewire at the intersection of the three surfaces defining the X-ray beam corresponding to the guidewire on the three 2-D images. Fig. 1 illustrates this reconstruction process. This task is automated using an in-house developed software.
- 4) Guidewire Position Error Estimation: The 3-D position error between intraoperative guidewire points and simulated guidewire nodes is measured using the Hausdorff Distance (HD) and the Modified Hausdorff Distance (MHD) [23]. For the two sets of points defining the real guidewire $G_{\rm real}$ and the simulation guidewire $G_{\rm simu}$, the HD and MHD are defined by

$$\text{HD } (G_{\text{real}}, G_{\text{simu}}) = \max \left[\max_{p \in S_{\text{real}}} d\left(p, G_{\text{simu}}\right), \right. \\ \left. \max_{p \in S_{\text{simu}}} d\left(p, G_{\text{real}}\right) \right]$$
 (5)
$$\text{MHD } (G_{\text{real}}, G_{\text{simu}}) = \max \left[\max_{p \in S_{\text{real}}} d\left(p, G_{\text{simu}}\right), \right. \\ \left. \max_{p \in S_{\text{simu}}} d\left(p, G_{\text{real}}\right) \right]$$
 (6)

The distance d(p, G) corresponds to the minimal distance between a point p and a set of points G and is defined by

$$d(p,G) = \min_{x \in G} ||p - x|| \tag{7}$$

where ||.|| denotes to the Euclidian norm.

The value of $d(p,G_{\rm real}),\ p\in G_{\rm simu}$ corresponds to the minimal distance to the real guidewire along the path of simulation guidewire. It reflects the local distribution of the position error along the guidewire path. The HD represents the maximum value of this local error along the guidewire path and the MHD represents its average value. The calculations are done with scripts developed with the software MATLAB (R2014a, The MathWorks, Natick, MA, USA).

D. Target Level of Accuracy

No gold standard exists regarding the level of acceptable error for guidewire simulations. Usually stent-graft manufacturers recommend a margin of 5–10 mm for length sizing of stent-graft modules, but this limit is hardly transposable in term of error on guidewire position. Therefore, we define several thresholds based on uncertainty estimations and discussions with the surgical staff.

In this study, simulation results are compared to snapshots taken during the intervention. The observation of fluoroscopy sequences of several seconds shows that, in reality, arteries and tools can be subjected to small displacements due to respiration and heart motion or possible movements of the surgeon. To estimate the uncertainty of the measure due to these motions, on one patient case, we were able to extract two 3-D positions of the guidewire approximately 10 s apart and compute the distance between these two positions. The MHD amounted to around 3 mm, which gives an estimation of the measure uncertainty for the intraoperative guidewire position.

The error measured through MHD encompasses the simulation error but also the possible error due to the registration step. This may be the consequence of inter-/intra-operator variability, intrinsic uncertainty of the registration method, reconstruction process, but also from a change in rachis position or aneurysm evolution between the preoperative CT-scan and the intervention. To account for the whole uncertainty of the measure, a threshold of 5 mm in terms of MHD is defined as the lowest attainable limit of accuracy. Below this threshold, the measured error is under the sensitivity threshold of the comparison method. Then, in accordance with clinicians, a threshold of 10 mm in terms of HD is adopted as the limit below which the result are deemed acceptable for clinical purposes. This threshold will have to be adjusted depending on future specific target applications.

E. Quantification of Simulation Contribution

Today, stent-graft sizing or intraoperative fusion roadmap are based on the preoperative CT-scan geometry only. We want to estimate the gain in accuracy for the prediction of the intraoperative guidewire position based on the simulation results compared to the preoperative configuration, which is the current gold

Patient	Case	Age	Sex	Side of introduction	Iliac tortuosity	Iliac calcification	Thrombus thickness (mm)	Aortic angulation (°)	Luminal Volume (mm ³)
1	1	73	M	Right	1.25	16%	10	128	130
2	2	78	M	Left	1.53	15%	20	138	117
3	3	67	M	Left	1.36	2%	24	131	211
4	4	79	M	Right	1.34	62%	10	157	106
5	5	77	M	Left	1.39	2%	28	130	118
6	6	75	M	Left	1.24	20%	25	148	103
7	7	81	M	Left	1.40	3%	0	148	119
7	8	81	M	Right	1.46	0%	0	148	119
8	9	80	M	Right	1.27	15%	38	158	75
9	10	88	M	Left	1.57	16%	15	141	108
10	11	70	M	Left	1.20	8%	18	154	117
11	12	78	M	Left	1.34	10%	26	152	97
12	13	65	M	Right	1.18	10%	10	155	175
13	14	64	M	Left	1.51	5%	20	150	215
13	15	64	M	Right	1.71	2%	20	150	215
14	16	72	M	Left	1.52	1%	10	153	119
15	17	80	F	Right	1.25	63%	0	143	75
16	18	85	M	Right	1.46	49%	20	109	117
17	19	67	M	Right	1.09	14%	14	141	98
18	20	64	M	Right	1.22	4%	21	159	144
19	21	92	M	Left	1.64	9%	22	169	74
20	22	80	F	Right	1.31	9%	0	142	85
21	23	74	M	Left	1.22	9%	10	142	110
22	24	59	M	Left	1.23	61%	15	164	110
23	25	56	M	Right	1.26	8%	10	156	107
24	26	75	M	Right	1.48	23%	24	139	115
25	27	79	M	Left	1.41	10%	7	154	104
26	28	79	M	Right	1.44	24%	0	134	96
27	29	67	M	Right	1.31	19%	22	159	85
28	30	66	M	Right	1.25	26%	10	150	104
	mean standard deviation min				1.37	17%	15	147	119
					0.15	18%	9.6	12	38
					1.09	0%	0	109	74
			max		1.71	63%	38	169	215

TABLE I
CLINICAL AND MORPHOLOGICAL SUMMARY

standard. The arterial centerline of the aorto-iliac axis, denoted $C_{\rm preop}$, is defined as the neutral reference of the preoperative configuration. We compute the MHD between this line and the real intraoperative guidewire $(G_{\rm real})$ to estimate the error made based on the preoperative configuration. This error is compared to the simulation error defined by the MHD between the simulation guidewire $(G_{\rm simu})$ and the real intraoperative guidewire. Finally, the gain in precision is defined as the relative difference between these two quantities expressed in percentage:

$$gain = \frac{\text{MHD}(C_{\text{preop}}, G_{\text{real}}) - \text{MHD}(G_{\text{simu}}, G_{\text{real}})}{\text{MHD}(C_{\text{preop}}, G_{\text{real}})} \times 100.$$
(8)

F. Calibration and Validation

A sensitivity study performed on one patient case in a previous work [12] showed the aorto-iliac support stiffness is the most influential feature in the model. In this study, we keep other modeling parameters (material, thickness) to average values proposed in [12] and we adjust the support's parameters $\{k_{\max}, d_{\max}, sf_a, sf_c, sf_s\}$ to calibrate the model.

As the number of parameters is important and the simulation time is long, the calibration cannot be done with standard automatic optimization methods. As a first step, in this study we use anatomical observations and experience gained through comparison of simulation results to the intraoperative reality to estimate realistic values for these parameters. This set of parameters is then applied on the 28 patient cases as a blinded evaluation. The calibration and the validation results are reported in Part III.

III. RESULTS

The vascular anatomies of the 28 cases were analyzed, and the five anatomical descriptors described in Section II-B were computed. For two patients, intraoperative acquisition was done with introduction of one guidewire in each iliac artery; for these patients, we report tortuosity index and calcification percentage for both sides. Table I reports the computed factors along with the side of introduction of the guidewire for the 28 patients, with mean, standard deviation, minimum and maximum values. Computed values showed the important anatomical variability of the population. In EVAR recommendations, iliac tortuosity is graded as: absent below 1.25, mild between 1.25 and 1.5, moderate between 1.5 and 1.6, and severe above 1.6. Arterial angulations are graded as absent over 150°, mild between 150° and 135°, moderate between 135° and 120°, and severe if the angle lower than 120°. For the three other indicators, no standard grading system were directly applicable; however, we noted the presence of moderate to severe cases with:

TABLE II SUPPORT PARAMETERS

Abdominal aorta	Common iliac arteries	External iliac arteries
$ \frac{\{sf_a, sf_c, sf_s\}}{\{0.25, 1, 0.25\}} $	$egin{array}{l} \{sf_a, sf_c, sf_s\} \ = \{0, 0.25, 0\} \ m{k_{max}} = 0.001 \ m{MPa/mm} \ m{d_{max}} = 30 \ m{mm} \end{array}$	$ \begin{cases} sf_a, sf_c, sf_s \\ $

- 1) six cases presenting high *tortuosity index* superior to 1.5;
- 2) five cases presenting *aortic angle* below 135°;
- four cases presenting an iliac calcification percentage superior to 30%;
- 4) nine cases presenting a maximal *thrombus thickness* superior to 2 cm; and
- 5) two cases presenting a *luminal volume* greater than 200 mm³.

A. Calibration

- 1) The parameter $d_{\rm max}$ represents the distance of effect of spine support. A realistic value for it is about the normal diameter of the aorta. After some observations, we set its value to 30 mm.
- 2) The value of $k_{\rm max} = 0.001$ MPa/mm was determined based on the sensitivity analysis proposed in [12]. Then, the stiffness of the support along the various segments of the vascular structure is modulated thanks to the anisotropy factors $\{sf_a, sf_c, sf_s\}$.
- 3) External iliacs are very movable parts and weakly attached to bones structures, we assumed that support stiffness can be neglected on these portions: $sf_a = sf_c = sf_s 0$
- 4) Common iliacs are mostly constraint in the sagittal direction by the proximity of the rachis. The factor sf_s was set to 0.25 and the axial and coronal anisotropy factors $sf_a = sf_c$ were chosen null on these parts.
- 5) Along the abdominal aorta, the factor sf_c was set to 1 to account for the strong tethering of the spine, the factors sf_a and sf_s were set to 0.25 to allow sliding between the aorta and the spine.

The final parameters set used for the simulations is summed up Table II. The resulting distribution of elastic stiffness along the vascular structure is illustrated Fig. 2.

B. Validation

Simulation was successfully conducted on the 28 patients, resulting in 30 configurations of deformed vascular structure and guidewire. Table III reports the results of comparison to intraoperative data for the 30 simulations given by values of MHD, HD and gain. The mean position error given by MHD for the 30 cases was 3.8 mm (± 1.9 mm), which demonstrates very good results for most of the cases. More precisely, for 22 cases the position error given by MHD was lower than 5 mm, which was defined as the lowest attainable level of accuracy.

TABLE III
COMPARISON RESULTS

Case	Side	MHD (mm)	HD (mm)	Gain (%)
1	Left	2.7	5.4	78
2	Right	2.0	4.2	82
3	Left	8.8	17	29
4	Right	3.1	4.1	67
5	Left	5.2	8.2	60
6	Left	2.3	5.1	81
7	Left	6.2	10	59
7	Right	2.7	6.9	84
8	Right	4.7	7.4	54
9	Left	5.1	13	57
10	Left	4.7	11	54
11	Left	5.7	7.4	57
12	Right	2.9	4.7	69
13	Left	4.6	8.0	69
13	Right	3.0	6.7	83
14	Left	2.1	3.4	85
15	Right	1.7	3.7	85
16	Right	8.0	12	16
17	Right	3.2	6.3	62
18	Right	3.7	7.8	66
19	Left	3.8	6.1	68
20	Right	2.9	5.3	77
21	Left	3.6	7.1	64
22	Left	2.5	5.0	55
23	Right	5.8	8.5	51
24	Right	1.3	3.5	86
25	Left	6.6	9.8	51
26	Right	2.1	2.9	65
27	Right	2.1	4.0	80
28	Right	2.3	3.6	72
n	nean	3.8	6.8	66
standar	d deviation	1.9	3.3	16

Only four cases showed a value of HD greater than 10 mm, which was defined as the level of acceptable error for clinical use, these cases are discussed in Part IV. The computed values of the *gain* showed that for all cases the deformed configuration given by the simulation was closer to the intraoperative reality than the undeformed preoperative configuration. For the two cases, presenting the highest MHD (patients 3 and 16) the *gain* was relatively low, yet for all other cases we observed a precision improvement with a *gain* value from 51% to 86% and a mean value of 69% (\pm 16). The comparison of the simulation guidewire to the intraoperative guidewire along with the initial and the deformed vascular structure are illustrated for the 28 cases (see Figs. 3–5). The colormap represents the distribution of local position error along the path of the simulation guidewire.

IV. DISCUSSION

In this research, we presented the evaluation on 30 cases of a finite-element mechanical simulation of the insertion of an extrastiff guidewire into an aorto-iliac structure that was developed in a previous work [12]. The quality of the simulation results was evaluated based on the guidewire position accuracy, assessed by MHD and HD. The computation of the *gain* gives an estimation of the accuracy improvement for intraoperative configuration prediction compared with the only currently available configuration, which is the preoperative CT-scan. The results showed that despite the high variability of vascular morphologies, the

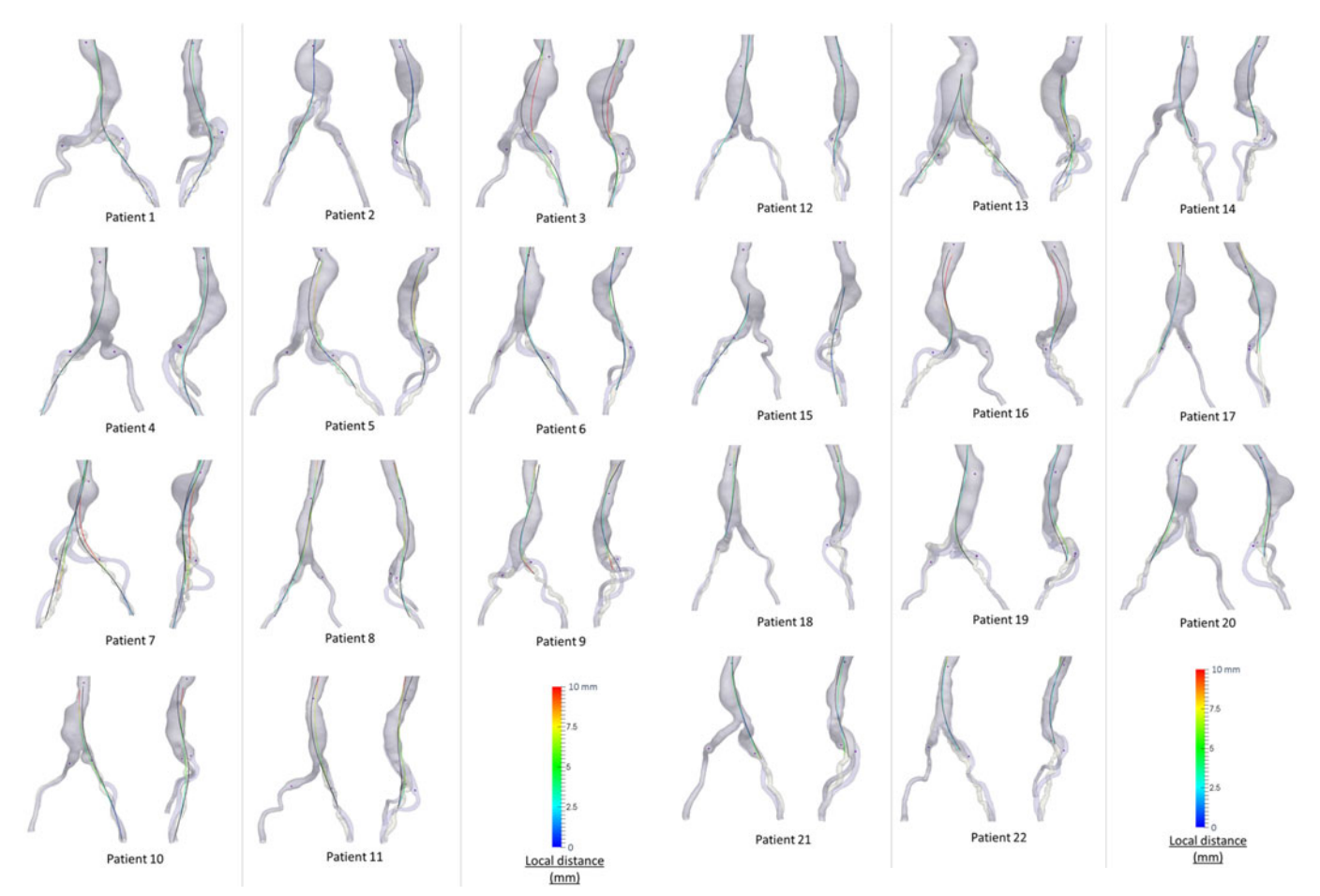


Fig. 3. Comparison between simulation and intraoperative guidewire for patients 1–11. Light purple: initial vascular structure mesh, Light gray: deformed vascular structure mesh. Black line: intraoperative guidewire. Color line: local position error along the simulation guidewire. Points corresponding to the limits of the area of interest for the comparison (most distal renal artery to internal iliac artery) are represented by purple spheres.

model is able to predict the final deformed configuration of vessels and guidewire with good accuracy with a parametrization common to all patients. Even for the less accurate cases, the value of *gain* was above 15%, which reflects the positive contribution of the simulation.

A. High Error Cases

Among the 30 studied cases, only four of them showed a HD value higher than 10 mm. For patients 3 and 16, the simulation guidewire appeared globally less curved than the real intraoperative one. These two patients presented an acute *aortic angle*. As in the standard protocol preoperative CTA images extend only up to descending aorta, the aorta was not represented over its full length in the models. Thus, the guidewire was left free at its upper end, whereas in reality it should be constrained inside the aortic arch, generating a nonnegligible bending moment at its upper extremity. As this condition was not taken into account, the guidewire may not have been able to constrain to a shape as curved as what is observed on the real intraoperative one. This effect is accentuated in the case of important aortic angulations.

Fig. 4. Comparison between simulation and intraoperative guidewire for patients 12–22.

Moreover, patient 3 presented a high aneurysm volume. According to our experience, for this kind of cases, the guidewire is less constrained inside the lumen and may take several different equilibrium positions depending, for instance, on boundary conditions imposed at its extremities, like the angle imposed by the surgeon at the distal insertion site or the insertion depth inside the aortic arch, this may explain the important deviation observed here.

For patients 9 and 10, the maximum of local error was located at the upper and lower limits of the area of interest, but in both the cases the mean error given by the MHD remained in the order of 5 mm, which demonstrates a good accuracy along the main portion of the guidewire path. This important level of error at the extremities can be the result of incorrect representation of boundary conditions, respectively, at the insertion point or in the aortic arch. To minimize the error due to the conditions of insertion, in each of the 28 patient cases, the angle and the depth of insertion of the guidewire were evaluated on intraoperative images to reduce the deviation a the distal end before running the blinded evaluation.

B. Limitations

Some simplifying modeling choices have been made. They may be sources of inaccuracy.

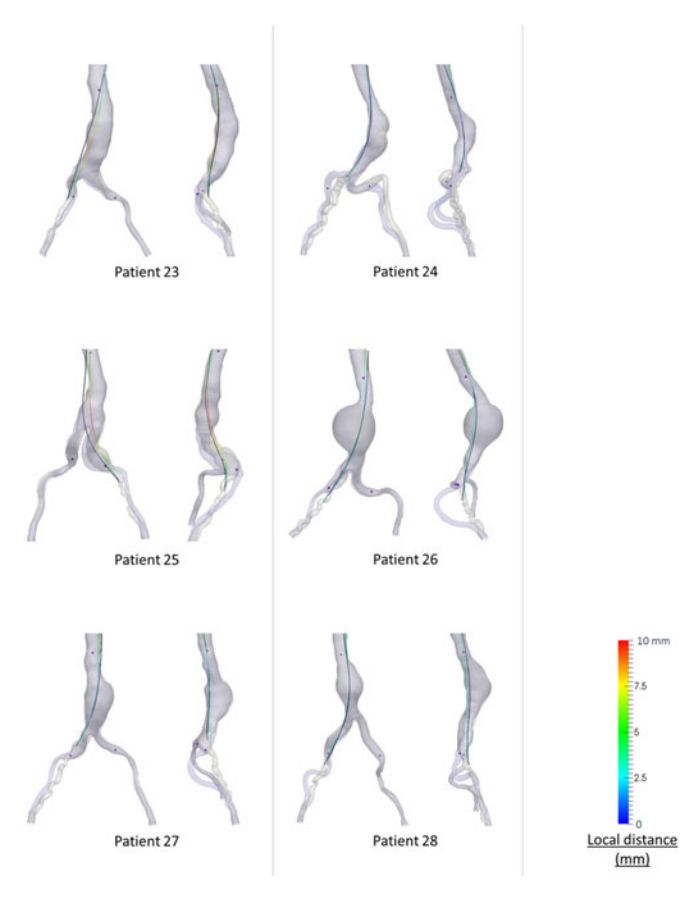


Fig. 5. Comparison between simulation and intraoperative guidewire for patients 23–28.

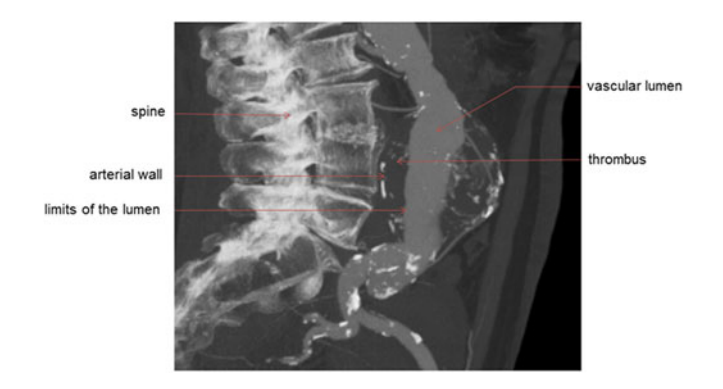


Fig. 6. Illustration of the presence of significant intraluminal thrombus.

1) The intraluminal thrombus, particularly in case of significant thickness, may play a part in the behavior of vascular structure [24], [25]. Even if its stiffness is far lower than the arterial wall ([26]–[28]), its important thickness provides bending rigidity to the wall, which is neglected in the model today. Moreover, when the thrombus is located on the posterior face of the aneurysm, the lumen limit is shifted away, whereas the arterial wall can still be in contact with the spine (see Fig. 6). In these kind of cases, the distance between the arterial wall and the spine is not correctly evaluated in the current model and may lead to an underestimated stiffness of the support.

2) In the present work, only the specific relative position between the wall and spine was included in the external support representation. Some soft tissues and organ may also play a less significant, but nonnegligible part in the vascular structure response. They may include the vena cava and iliac veins or digestive organs.

For instance, case 5, showed a relatively important simulation error (MHD = $5.2\,$ mm, HD = $8.2\,$ mm). This case presented an important intraluminal thrombus thickness ($28\,$ mm). Besides, in reality the iliac vein may have reduced possible motion of the left common iliac artery, which can explain the overestimated displacement of this segment observed in the simulation. To get a more precise representation of the external support, future developments should focus on the inclusion of the relative position of soft organs to the vascular structure along with the presence of thrombus. Yet, currently the robust segmentation of thrombus and soft tissues is still a matter of research and represents the main obstacle to their inclusion in mechanical models.

The validation study presented here demonstrates the accuracy of the simulation in terms of guidewire position. Observation of the vascular structure actually deformed by the guidewire during the procedure is technically more difficult. It implies a 3-D rotational acquisition synchronized with the injection of contrast agent, which raises the complexity and the duration of the surgical procedure and substantially increases the dose of radiation and iodine received by the patient [5], [29]. Besides, the data cannot be used directly for comparison with the simulation, in particular, because the quality of the images obtained by this process does not allow automatic segmentation of the lumen, this is why this kind of data was not used in the present study. Future investigations should focus on validation based on vascular structure comparison, which can involve use of 2-D and 3-D angiographic images [5] but also non-injected images with the use of radio-opaque anatomical markers like calcification plaques.

The simulation was run with the same set of parameters for the 28 patients. At this stage, we cannot state that this set of parameters would give the same accuracy on a new population of patients. Yet, 28 patients constitute a relatively large cohort for this kind of study, and the included cases were chosen to represent wide morphological variations that exist in the patients' population as attested by the provided morphological descriptors, so we can optimistically believe that the results would not be significantly different on a new cohort. Nevertheless, a larger validation study would be needed before the simulation can be used as clinical decision-support tool.

C. Clinical Applications

In this study, we aimed at verifying the predictability of the model in terms of guidewire position. The possible clinical applications of the simulation are not demonstrated, and will be the subject of a future work. But this work represents a first step toward clinically validated simulations.

The primary aim of the simulation is to predict the intraoperative configuration of the vascular structure deformed by the stiff wires and could be easily extended to other devices (delivery systems, introducers). This deformed configuration may be

used at two levels. First, at the planning step, to improve stent-graft sizing by anticipating changes of lengths and angulations. Then, during the procedure, to update the intraoperative fusion which, today, is often called into question once stiff devices have deformed the vascular structure.

Second, the model developed and validated here could be used to estimate risks associated with iliac access. Indeed, as part of the strategy planning, the clinician must also ensure that the patient's anatomy is favorable to EVAR and, particularly, that guidewires will be able to straighten enough iliac arteries to enable access of the stent-graft modules to the deployment site [30]. If not, conventional open surgery may be preferred. Complication risks related to iliac access include arterial wall damage, dissection, or even impossibility to insert the stent-graft delivery system; they are often associated with high tortuosity, important calcification, and low diameter of external iliac arteries [31], [32]. Some guidelines exist based on morphology grading to evaluate the access-related complications risk from direct analysis of CTA data [15]. But these grades rely primary on the surgeon appreciation and are not always able to account for the specificity of each anatomy or device used. Future work should aim at investigating possible risk indicators:

- 1) guidewire curvature can indicate a risk of impossibility to deliver the stent-graft as proposed in [33] and
- reaction forces generated on the wire during its insertion or strain and stress levels in the arterial wall could give indicators of damage risk.

Finally, the possibility to predict the postoperative mechanical equilibrium between the vascular structure and the stent-graft is a major research topic [10], [13], [14]. Such a mechanical model could provide information on complications risks like endoleaks, migration, kinking, and occlusion [34] and, therefore, be a powerful clinical decision-support tool. It also opens prospects for stent-graft manufacturers as a valuable tool to develop and optimize stent design. To our knowledge, the work presented here offers the first numerical framework for tools insertion on a whole femoral to aortic arch vascular structure taking into account blood pressure pretension and external support modeling, and is, therefore, a first step toward the simulation of the complete process of stent-graft deployment.

V. CONCLUSION

The work reported here shows that numerical simulation can predict some rather large variations in the vascular geometry due to tools insertion, for a wide variety of aorto-iliac morphologies even in the most severe cases. The validation method presented here is based on the guidewire position only. At this stage, we do not demonstrate that the model is fully ready and validated to be used as a clinical decision-support tool or to improve fusion guidance. However, even in the worst cases where the simulation error seems high, the predicted deformed configuration is still much closer to the intraoperative deformed shape than the initial preoperative geometry. Thus, it should be more accurate for length measurements and intraoperative fusion. Future work should aim at verifying that a good prediction of the guidewire position demonstrated in this study implies a similar goodness

on the vascular structure deformed configuration prediction, to help sizing and fusion guidance. Further developments and investigations will focus on indicators of iliac access risks and complete stent-graft deployment simulations.

ACKNOWLEDGMENT

This work has been partially conducted in the experimental platform TherA-Image (Rennes, France) supported by Europe FEDER. This study has been partially supported by the French National Research Agency (ANR) in the context of the Endosim project (grant n° ANR-13-TECS-0012). The authors gratefully thank Aurelien Dumenil (Therenva) for his help and development of 3-D reconstruction and registration applications used in this study.

REFERENCES

- P. Markelj et al., "A review of 3D/2D registration methods for imageguided interventions," Med. Image Anal., vol. 16, no. 3, pp. 642–661, Apr. 2012.
- [2] A. Kaladji et al., "Safety and accuracy of endovascular aneurysm repair without pre-operative and intra-operative contrast agent," Eur. J. Vasc. Endovasc. Surg., vol. 49, no. 3, pp. 255–261, Mar. 2015.
- [3] L. Stangenberg et al., "A novel tool for three-dimensional roadmapping reduces radiation exposure and contrast agent dose in complex endovascular interventions," J. Vasc. Surg., vol. 62, pp. 448–455, Jun. 2015.
- [4] G. Koutouzi et al., "EVAR guided by 3D image fusion and CO2 DSA: A new imaging combination for patients with renal insufficiency," J. Endovasc. Ther., vol. 22, no. 6, pp. 912–917, 2015.
- [5] B. Maurel et al., "Evaluation of visceral artery displacement by endograft delivery system insertion," J. Endovasc. Ther., vol. 21, no. 2, pp. 339–347, Apr. 2014.
- [6] A. M. Sailer et al., "CTA with fluoroscopy image fusion guidance in endovascular complex aortic aneurysm repair," Eur. J. Vasc. Endovasc. Surg. Off. J. Eur. Soc. Vasc. Surg., vol. 47, no. 4, pp. 349–356, Apr. 2014.
- [7] C. Kauffmann et al., "Source of errors and accuracy of a twodimensional/three-dimensional fusion road map for endovascular aneurysm repair of abdominal aortic aneurysm," J. Vasc. Interv. Radiol., vol. 26, no. 4, pp. 544–551, 2015.
- [8] A. Kaladji et al., "Prediction of deformations during endovascular aortic aneurysm repair using finite element simulation," Spec. Issue Mix. Real. Guid. Ther.—Clin. Implement., vol. 37, no. 2, pp. 142–149, Mar. 2013.
- [9] G. Mouktadiri et al., "Aortic endovascular repair modeling using the finite element method," J. Biomed. Sci. Eng., vol. 6, no. 9, pp. 917–927, Sep. 2013.
- [10] D. Roy et al., "Finite element analysis of abdominal aortic aneurysms: geometrical and structural reconstruction with application of an anisotropic material model," IMA J. Appl. Math., vol. 79, no. 5, pp. 1011–1026, Oct. 2014.
- [11] A. Dumenil *et al.*, "Finite-element-based matching of pre- and intraoperative data for image-guided endovascular aneurysm repair," *IEEE Trans. Biomed. Eng.*, vol. 60, no. 5, pp. 1353–1362, May 2013.
- [12] J. Gindre et al., "Finite element simulation of the insertion of guidewires during an EVAR procedure: Example of a complex patient case, a first step toward patient-specific parameterized models," Int. J. Numer. Methods Biomed. Eng., vol. 31, 2015.
- [13] S. De Bock et al., "Virtual evaluation of stent graft deployment: A validated modeling and simulation study," J. Mech. Behav. Biomed. Mater., vol. 13, pp. 129–139, Sep. 2012.
- [14] D. Perrin et al., "Patient-specific numerical simulation of stent-graft deployment: Validation on three clinical cases," J. Biomech., vol. 48, no. 10, pp. 1868–1875, Jul. 2015.
- [15] E. L. Chaikof et al., "Identifying and grading factors that modify the outcome of endovascular aortic aneurysm repair," J. Vasc. Surg., vol. 35, no. 5, pp. 1061–1066, May 2002.
- [16] G. T. Walker et al., "Clinical practice guidelines for endovascular abdominal aortic aneurysm repair: Written by the standards of practice committee for the society of interventional radiology and endorsed by the cardiovascular and interventional radiological society of europe and the canadian interventional radiology association," J. Vasc. Interv. Radiol., vol. 21, no. 11, pp. 1632–1655, Nov. 2010.

- [17] J. Bols et al., "A computational method to assess the in vivo stresses and unloaded configuration of patient-specific blood vessels," J. Comput. Appl. Math., vol. 246, pp. 10–17, 2013.
- [18] F. Riveros *et al.*, "A pull-back algorithm to determine the unloaded vascular geometry in anisotropic hyperelastic AAA passive mechanics," *Ann. Biomed. Eng.*, vol. 41, no. 4, pp. 694–708, Apr. 2013.
- [19] A. Gupta et al., "Investigation of interaction between guidewire and native vessel using finite element analysis," in Proc. Simulia Customer Conf., 2010
- [20] A. Duménil, A. Kaladji, M. Castro, C. Göksu, A. Lucas, and P. Haigron, "A versatile intensity-based 3D/2D rigid registration compatible with mobile C-arm for endovascular treatment of abdominal aortic aneurysm," *Int. J. Comput. Assist. Radiol. Surg.*, pp. 1–17, 2016.
- [21] S. A. M. Baert *et al.*, "Three-dimensional guide-wire reconstruction from biplane image sequences for integrated display in 3-D vasculature," *IEEE Trans. Med. Imag.*, vol. 22, no. 10, pp. 1252–1258, Oct. 2003.
- [22] T. van Walsum *et al.*, "Guide wire reconstruction and visualization in 3DRA using monoplane fluoroscopic imaging," *IEEE Trans. Med. Imag.*, vol. 24, no. 5, pp. 612–623, May 2005.
- [23] M.-P. Dubuisson and A. K. Jain, "A modified Hausdorff distance for object matching," in *Proc. 12th IAPR Int. Conf. Pattern Recognit. vol. 1, Conf. Comput. Vis. Image Process.*, 1994, vol. 1, pp. 566–568.
- [24] D. H. J. Wang et al., "Effect of intraluminal thrombus on wall stress in patient-specific models of abdominal aortic aneurysm," J. Vasc. Surg., vol. 36, no. 3, pp. 598–604, Sep. 2002.
- [25] F. Riveros et al., "Influence of intraluminal thrombus topology on AAA passive mechanics," in *Proc. Comput. Cardiol. Conf.*, Sep. 2013, pp. 899–902.
- [26] J. P. Vande Geest *et al.*, "A planar biaxial constitutive relation for the luminal layer of intra-luminal thrombus in abdominal aortic aneurysms," *J. Biomech.*, vol. 39, pp. 2347–2354, 2006.

- [27] J. Tong et al., "Effects of age on the elastic properties of the intraluminal thrombus and the thrombus-covered wall in AAA: Biaxial extension behaviour and material modelling," Eur. J. Vasc. Endovasc. Surg., vol. 42, pp. 207–219, 2011.
- [28] S. A. O'Leary et al., "The biaxial mechanical behaviour of abdominal aortic aneurysm intraluminal thrombus: Classification of morphology and the determination of layer and region specific properties," J. Biomech., vol. 47, no. 6, pp. 1430–1437, Apr. 2014.
- [29] A. Hertault et al., "Benefits of Completion 3D Angiography Associated with Contrast Enhanced Ultrasound to Assess Technical Success after EVAR," Eur. J. Vasc. Endovasc. Surg., vol. 49, no. 5, pp. 541–548, May 2015.
- [30] M. Tillich et al., "Iliac arterial injuries after endovascular repair of abdominal aortic aneurysms: correlation with iliac curvature and diameter," Radiology, vol. 219, no. 1, pp. 129–136, Apr. 2001.
- [31] J. P. Henretta et al., "Special iliac artery considerations during aneurysm endografting," Amer. J. Surg., vol. 178, no. 3, pp. 212–218, Sep. 1999.
- [32] Y. G. Wolf et al., "Impact of aortoiliac tortuosity on endovascular repair of abdominal aortic aneurysms: Evaluation of 3D computer-based assessment," J. Vasc. Surg., vol. 34, no. 4, pp. 594–599, Oct. 2001.
- [33] V. J. Gokani et al., ""Trial of stiff guidewire": A useful adjunct to determining suitability for endovascular aneurysm repair," Eur. J. Vasc. Endovasc. Surg., vol. 44, no. 5, p. 527, Nov. 2012.
- [34] H.-E. Altnji et al., "Morphological and stent design risk factors to prevent migration phenomena for a thoracic aneurysm: A numerical analysis," Med. Eng. Phys., vol. 37, no. 1, pp. 23–33, Jan. 2015.

Authors' photographs and biographies not available at the time of publication.